JACS
JOURNAL OF THE AMERICAN CHEMICAL SOCIETY
Article
Cite This: J. Am. Chem. Soc. 2019, 141, 17015−17021
pubs.acs.org/JACS

Quadruply B←N-Fused Dibenzo-azaacene with High Electron Affinity and High Electron Mobility

Yang Min,[†,§] Chuandong Dou,*[,†] Dan Liu,[‡,§] Huanli Dong,*[,‡] and Jun Liu*[,†]

[†]State Key Laboratory of Polymer Physics and Chemistry, Changchun Institute of Applied Chemistry, Chinese Academy of Sciences, Changchun 130022, P.R. China

[‡]Beijing National Laboratory for Molecular Science, Key Laboratory of Organic Solids, Institute of Chemistry, Chinese Academy of Sciences, Beijing 100190, P.R. China

[§]University of Chinese Academy of Sciences, Beijing 100049, P.R. China

Supporting Information

ABSTRACT: For many years, organoboron compounds have been expected to show excellent electron-injecting and -transporting properties. However, lowest unoccupied molecular orbital (LUMO) energy levels (E_{LUMO}) of B-containing π-conjugated molecules are mostly higher than −4.0 eV and their electron mobilities are usually less than 10^{-2} cm^2 V^{-1} s^{-1}. In this work, we experimentally prove the remarkably high electron affinity and high electron mobility of organoboron compounds. Our strategy is to incorporate multiple boron−nitrogen coordination bonds (B←N) into azaacenes. We synthesized quadruply B←N-fused dibenzo-azaacene (**QBNA**) through one-pot multifold borylation cyclization reaction. The incorporation of four B←N units greatly changes the electronic structures and properties and significantly downshifts the electronic energy levels of **QBNA**. **QBNA** shows a E_{LUMO} of as low as −4.58 eV, which is among the lowest for n-type organic semiconductors. Single-crystal organic field-effect transistors of **QBNA** display unipolar n-type characteristic with an electron mobility of up to 1.60 cm^2 V^{-1} s^{-1} together with excellent ambient stability. This study thus provides a design strategy for high-performance n-type organic semiconductors and high electron-affinity π-systems based on organoboron chemistry.

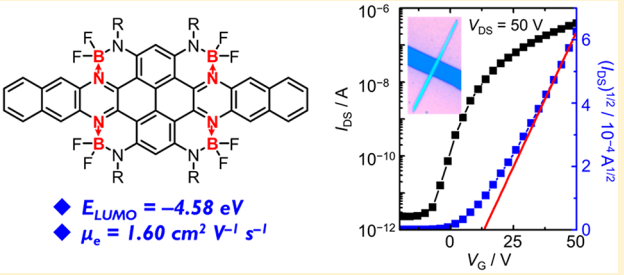

INTRODUCTION

A fundamental characteristic of π-electron systems and π-conjugated materials is electron affinity.[1] High electron affinity, which is generally characterized by low-lying LUMO energy level (E_{LUMO}), leads to various intriguing properties of π-systems, such as easy electron injection, stable electron transport, strong electron acceptor, and facilitated n-type doping.[2] Therefore, π-systems with high electron affinity have drawn much attention in both synthetic chemistry and organic electronic materials. The general strategy to design molecules with high electron affinity is to incorporate the electron-withdrawing units, such as imide unit, halogen atoms (Cl and F), cyano group, and sp^2-hybridized N atom (Figure 1a).[3] However, as π-systems are intrinsically electron-rich, it is challenging to develop π-conjugated molecules with extremely high electron affinity (low E_{LUMO}).

A particular application of π-conjugated molecules with high electron affinity is as n-type semiconductors in organic field-effect transistors (OFETs).[4] High electron affinity of n-type organic semiconductors (E_{LUMO} < ca. −4.0 eV) can enable efficient electron injection and good ambient stability of OFETs. Integrating multiple electron-withdrawing units onto large π-frameworks has been proved to be efficient to produce high-performance n-type organic semiconductors.[5] However, it is very difficult to design and synthesize them. Only a few n-type organic semiconductors with high electron mobilities (μ_e) and good stability have been developed, such as aromatic diimides, tetraazapentacenes, benzodifurandione-based oligo-

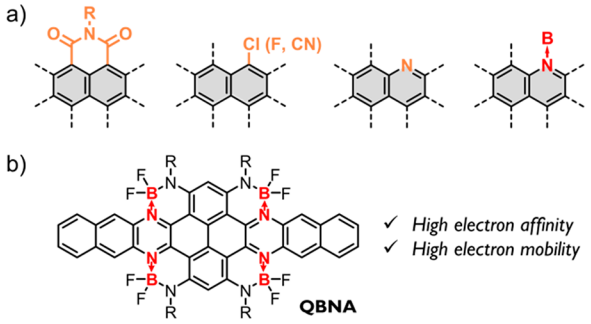

Figure 1. (a) Examples of molecular segments with high electron affinity, which are based on imide unit, halogen atoms, cyano group, sp^2-hybridized N atom, and B←N unit. (b) Chemical structure of quadruply B←N-fused dibenzo-azaacene (**QBNA**).

Received: September 6, 2019
Published: October 2, 2019

Downloaded via TIANJIN UNIV on January 10, 2024 at 08:45:25 (UTC).
See https://pubs.acs.org/sharingguidelines for options on how to legitimately share published articles.

© 2019 American Chemical Society

DOI: 10.1021/jacs.9b09640
J. Am. Chem. Soc. 2019, 141, 17015−17021

Scheme 1. Synthesis of 5a and 5b[a]

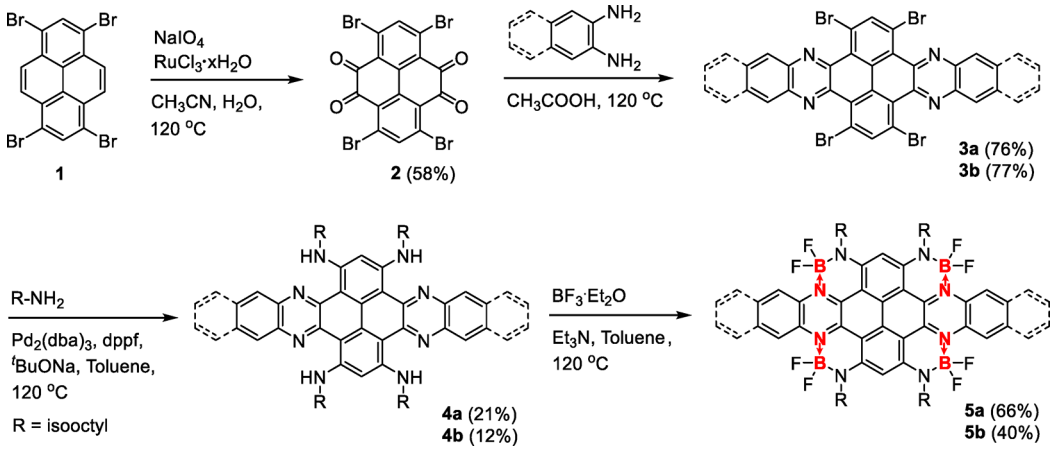

[a]**3a**−**5a**: Six linearly annelated rings. **3b**−**5b**: Eight linearly annelated rings.

(*p*-phenylenevinylene), and cyano-containing quinoidal terthiophenes, as well as their derivatives, etc.[6] New n-type organic semiconductors with excellent OFET device performance thus remain important and attractive.

Boron atom has one less electron than carbon atom and has a typical empty p-orbital. This feature characterizes boron species as electron-deficient scaffolds that can induce intriguing optoelectronic properties of organoboron compounds,[7] such as two-photon absorption, near-infrared light absorption, thermally activated delayed fluorescence, etc.[8] For many years, incorporating B atoms into π-systems is expected to be an effective approach to accomplish high electron affinity and high electron mobility.[7,9] However, B-containing π-conjugated molecules seldom show adequately high electron affinity and their E_{LUMO} are usually higher than −4.0 eV. B-containing π-conjugated molecules also display unsatisfactory electron-transporting properties. Their electron mobilities are usually less than 10^{-2} cm^2 V^{-1} s^{-1}.[10] Boron species can coordinate with N-heteroaromatic rings to form boron−nitrogen coordination bond (B←N), which has led to various organic semiconductors and light-emitting materials.[11] Very recently, we developed a dibenzo-azaacene containing two B←N units, which shows a low-lying E_{LUMO} of −3.87 eV and a decent electron mobility of 0.21 cm^2 V^{-1} s^{-1}.[12] This study thus convinces us that B←N unit is a promising candidate to design π-conjugated molecules with high electron affinity and high electron mobility (Figure 1a).

In this work, we experimentally prove the remarkably high electron affinity and high electron mobility of organoboron compounds. This is realized by incorporating multiple B←N units into azaacene to design quadruply B←N-fused dibenzo-azaacene (**QBNA**). The incorporation of four B←N units greatly changes the electronic structures and properties and significantly downshifts the electronic energy levels of **QBNA**. **QBNA** shows an ultralow E_{LUMO} of −4.58 eV, which is among the lowest for n-type organic semiconductors. The single-crystal OFET (SC-OFET) devices based on **QBNA** display unipolar n-type characteristic with an electron mobility of up to 1.60 cm^2 V^{-1} s^{-1} and excellent ambient stability. To the best of our best knowledge, this is the first organoboron molecule with electron mobility higher than 1 cm^2 V^{-1} s^{-1}.

RESULTS AND DISCUSSION

Our synthetic strategy of the B←N-containing polyarenes is to perform a one-pot multifold borylation cyclization on the tetra-alkylaminated dibenzo-azaacenes. Scheme 1 illustrates the synthetic route of **QBNA** (**5b**) and its analog **5a**, which have eight and six linearly annelated rings, respectively. In the first step, oxidization of 1,3,6,8-tetrabromopyrene **1** using the conventional oxidization conditions for pyrene and its derivatives could lead only to the partially oxidized products.[13] So we improved the condition with $NaIO_4/RuCl_3{\cdot}xH_2O$ as the oxidant system and CH_3CN/H_2O as the solvent at a high reaction temperature of 120 °C, successfully producing the fully oxidized compound **2** in 58% yield. Condensation of **2** with benzene-1,2-diamine/naphthalene-2,3-diamine and then alkylamination of **3a**/**3b** produced the key precursors **4a**/**4b**, respectively. The moderate yields of the alkylamination step are due to the low solubility of **3a**/**3b**. Finally, the borylation reaction of **4a**/**4b** with $BF_3{\cdot}Et_2O/Et_3N$ afforded **5a**/**5b** in good yields, and in this step four B←N-fused six-membered rings are simultaneously formed. Notably, these B←N-containing polyarenes **5a** and **5b** are stable enough to be purified by silica gel column chromatography. They also show excellent light and oxygen stability as determined by the repeated photophysical measurements under ambient conditions in which no spectral change is observed. In addition, **5a** and **5b** are both well soluble in common organic solvents, such as chloroform, toluene, and tetrahydrofuran.

The structures of **5a** and **5b** were unambiguously confirmed by various NMR spectroscopies, high-resolution mass spectrometry, and elemental analysis (see Supporting Information). The ^{11}B NMR spectra exhibit only one signal at ca. 2.3 ppm (Figure S1). This is consistent with those for the organoboron compounds with boron atoms linked to two fluorines and two nitrogens and suggests that the four B←N units on the frameworks exist in the same manner.[14] In the ^{1}H NMR spectrum of **5b**, four different signals observed in the aromatic region reveal its 4-fold symmetric structure in solution. To assign H^a, H^b, and H^c in the backbone of **5b**, we also performed the ^{1}H−^{1}H COSY and 1D NOE measurements. In the ^{1}H−^{1}H COSY spectrum (Figure 2a), the correlation between H^a and H^b and no correlation of H^c (δ = 9.58 ppm, singlet) with others reveal that H^c is the proton adjacent to the B←N-linked ring. Two correlative signals in the 1D NOE

DOI: 10.1021/jacs.9b09640
J. Am. Chem. Soc. 2019, 141, 17015−17021

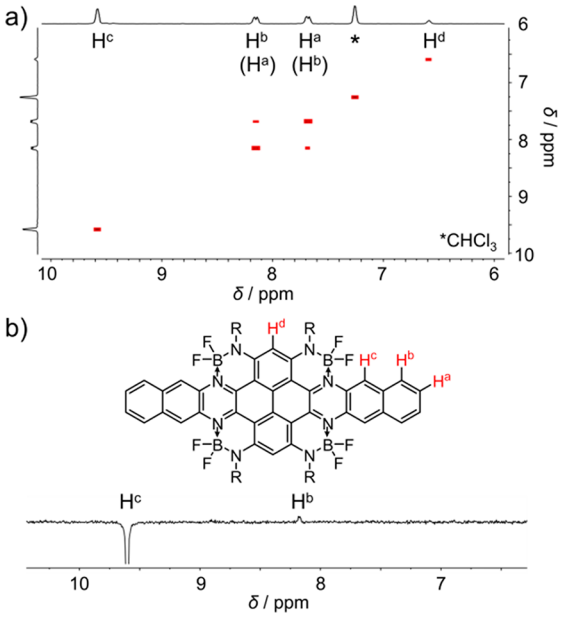

Figure 2. (a) $^{1}H-^{1}H$ COSY and (b) 1D NOE spectra of **5b**.

spectrum can assign H^b (δ = 8.16 ppm) to the proton close to H^c (Figure 2b).[15]

To gain insight into the configurations of **5a** and **5b**, we performed structural optimizations on the model compounds with methyl groups (**5a-Me** and **5b-Me**) using density functional theory (DFT) calculations (B3LYP/6-31G(d,p)). As shown in Figure 3 and Figure S4, **5a-Me** and **5b-Me** both

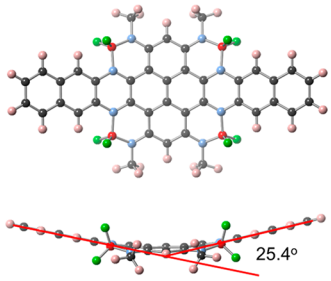

Figure 3. Optimized structure of **5b-Me** calculated at the B3LYP/6-31G(d,p) level.

adopt curved configurations along the azaacene skeletons with the dihedral angles of 23.4° and 25.4°, respectively. These curved configurations are in stark contrast to the planar configurations of the previously reported dibenzo-azaacenes containing two B←N units.[12] This is attributed to the incorporation of multiple B←N units in **5a** and **5b**, which results in large fused-ring strain of B←N-heterocycles and thus distorts the whole π-skeleton for strain relaxation. It is notable that this curved structure has no negative effects on molecular crystallinity. **5b** displays excellent crystallinity, which is beneficial for electron transport (vide infra). Recently, nonplanar polycyclic aromatic hydrocarbons (PAHs) have attracted great attention of synthesis chemists.[16] The general approach to design nonplanar PAH molecules is to incorporate non-six-membered rings or steric hindrance into π-skeletons. Inspired by this study and other recent reports,[17] the incorporation of B←N-containing six-membered cycles should be a new approach toward nonplanar PAHs.

Figure 4 shows the absorption spectra of **5a** and **5b** in toluene. **5a** shows two main absorption peaks (λ_{abs}) at 745/

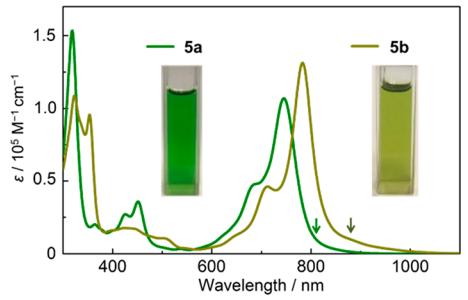

Figure 4. Absorption spectra of **5a** and **5b** in toluene. Insets are the photographs.

685 nm and a detectable weak band at 800 nm. **5b** exhibits two strong peaks at 783/712 nm and one weak band at 880 nm (Table 1 and Figure S5). Compared to that of **5a**, the absorption spectrum of **5b** is red-shifted by ca. 40 nm because of its extended π-conjugation. Electron-deficient polyarenes with large π-skeletons mostly exhibit the absorption maxima in the visible region. For example, a C_{64} nanographene containing four imides reported by Würthner and co-workers shows the λ_{abs} of 584 nm.[18a] A N-doped graphene nanoribbon with 7.7 nm in length reported by Mateo-Alonso and co-workers exhibits the λ_{abs} of 605 nm.[18b] In contrast, **5a** and **5b** containing four B←N units show the absorption peaks in the near-infrared (NIR) region. Moreover, the molar absorption coefficients of **5a** and **5b** are both as high as exceeding 1×10^5 M^{-1} cm^{-1}. The toluene solutions of **5a** and **5b** exhibit the green and yellowish green colors, respectively.

To elucidate these characteristic absorption bands, we conducted time-dependent DFT (TD-DFT) calculations on **5a-Me** and **5b-Me** at the B3LYP/6-31G(d,p) level (see Supporting Information). The calculation results are shown in Figure 5. For **5a**, while the weak absorption band at around

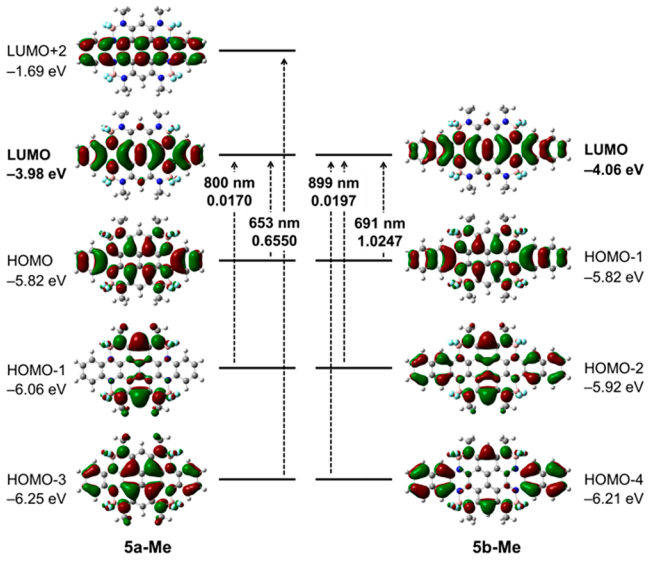

Figure 5. Selected Kohn−Sham molecular orbitals and energy diagrams of **5a-Me** and **5b-Me** calculated at the B3LYP/6-31G(d,p) level. Excitation energies and oscillator strengths were computed by TD-DFT at the same level.

DOI: 10.1021/jacs.9b09640
J. Am. Chem. Soc. 2019, 141, 17015−17021

Table 1. Summary of Optoelectronic Properties and Energy Levels of 5a and 5b

	λ_{abs} [a] [nm]	ε_{max} [a] [M^{-1} cm^{-1}]	E_g^{opt} [b] [eV]	$E_{1/2}^{red1}$ [c] [V]	$E_{1/2}^{red2}$ [c] [V]	$E_{1/2}^{red3}$ [c] [V]	E_{pa}^{ox} [c] [V]	E_{LUMO} [d] [eV]	E_{HOMO} [d] [eV]	E_g [e] [eV]
5a	745/685	1.07×10^5	1.57	−0.35	−0.90	−2.10	+1.14	−4.45	−5.94	1.49
5b	783/712	1.31×10^5	1.51	−0.22	−0.70	−1.94	+1.15	−4.58	−5.95	1.37

[a]In toluene solution (1×10^{-5} M). [b]Optical energy gaps calculated according to the equation $E_g^{opt} = 1240/\lambda_{onset}$ eV. [c]Half-reduction potentials and anodic peak potentials (vs Fc/Fc^+) measured in CH_2Cl_2 at a scan rate of 50 mV s^{-1}. [d]Estimated according to the equations $E_{LUMO}/E_{HOMO} = -(4.80 + E_{1/2}^{red1}/E_{pa}^{ox})$ eV. [e]Electrochemical gaps calculated according to the equation $E_g = (E_{pa}^{ox} - E_{1/2}^{red1})$ eV.

800 nm is assigned to the electronic transition of HOMO-1 → LUMO, the maximum absorption band at 600−800 nm is assigned to the HOMO → LUMO and HOMO-3 → LUMO +2 transitions. For **5b**, the weak absorption band at ca. 880 nm is attributed to the HOMO-4 → LUMO and HOMO-2 → LUMO transitions and the maximum absorption band is assigned to the HOMO-1 → LUMO transition. The absorption properties of **5a** and **5b** are well reproduced by the TD-DFT calculations. Accordingly, the weak absorption bands in the long-wavelength region of **5a** and **5b** are both attributed to the intramolecular charge transfer (ICT) transitions within π-frameworks accompanying small oscillator strengths (Figures S8 and S9). In addition, the absorption bands of **5a** and **5b** all involve their LUMOs. The LUMOs of **5a** and **5b** both are localized on the linear azaacene skeletons and the LUMO energy levels are very low (ca. −4.0 eV). These characteristics are totally different from those of the all-carbon analogous compounds (Figure S10). It is suggested that the four B←N units greatly perturb the electronic structures of π-skeletons, thus contributing to the NIR absorption properties of **5a** and **5b**.

To evaluate their electron affinity, we performed cyclic voltammetry measurements on **5a** and **5b** in CH_2Cl_2 using *n*-Bu_4NClO_4 (0.1 M) as supporting electrolyte. As shown in Figure 6, both of them exhibit three well-defined reversible

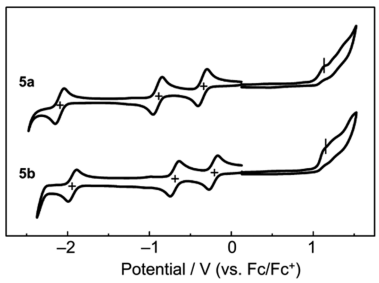

Figure 6. Cyclic voltammograms of **5a** and **5b** in CH_2Cl_2 (0.4 mM). Fc/Fc^+ = ferrocene/ferrocenium.

reduction processes, suggesting excellent stabilities of the generated radical anion intermediates. The half-reduction potentials ($E_{1/2}^{red}$) are −0.35/−0.90/−2.10 V for **5a** and −0.22/−0.70/−1.94 V for **5b** (Table 1), respectively (vs Fc/Fc^+). Irreversible oxidation processes are observed with the anodic peak potential (E_{pa}^{ox}) of +1.14 V for **5a** and +1.15 V for **5b**. On the basis of their first reduction and oxidation potentials, we estimated the LUMO and HOMO levels of **5a** and **5b**. The E_{LUMO} and E_{HOMO} are −4.45/−5.94 eV for **5a** and −4.58/−5.95 eV for **5b**, respectively. The ultralow E_{LUMO} of **5a** and **5b** experimentally prove their extremely high electron affinity. The variations in energy levels from **5a** to **5b** are fully consistent with the theoretical calculation results (Figure S11).

Low E_{LUMO} is necessary for efficient electron injection and transport of n-type organic semiconductors in OFETs.[4,5] The extremely low E_{LUMO} of ca. −4.5 eV of **5a** and **5b** are rarely achieved for B-containing π-systems. Only a few organoboron compounds show very low E_{LUMO}, which are mostly based on boron-dipyrromethene (BPDIPY), such as quinodimethane bridged BODIPY dimers and BF_2-containing bis-(pyrrolopyrrole) cyanines.[19] Compared to the reported dibenzo-azaacenes containing two B←N units, **5a** and **5b** containing four B←N units exhibit the lower E_{LUMO} by ca. 0.7 eV.[12] The extra two B←N units further lead to the large downshifts of the E_{LUMO} of π-systems. Moreover, the E_{LUMO} of **5a** and **5b** are among the lowest for the reported high-performance n-type organic semiconductors (Figure S13).[5] Therefore, the incorporation of multiple B←N units is an efficient strategy to significantly enhance electron affinity of the π-system.

Another interesting aspect is the crystalline property of **5b**. In our attempt to grow single crystals of these B←N-containing polyarenes in solution for X-ray structural analysis, we could obtain some micrometer-sized wires of **5b**. On the basis of this phenomenon, we prepared the microstructures of **5b** on the substrate via a solvent evaporation method. The solution of **5b** in toluene (1 mg/mL) was drop-casted on the octadecyltrichlorosilane (OTS)-treated SiO_2/Si substrate in a sealed Petri dish. After evaporation of the solvent, some microstructures appeared on the substrate. The polarized optical microscopy (POM) images in Figure 7a show that microwires with the length of around 20 μm are formed. When the substrate is rotated by 45°, these microwires exhibit the obvious color change from bright to dark, indicating the crystalline character of **5b**. As shown in Figure 7b, the atomic force microscopy (AFM) image of a typical microwire reveals a smooth surface with the thickness of around 36 nm. Transmission electron microscopy (TEM) and selected-area electron diffraction (SAED) were used to further assess the crystalline property of **5b**. As shown in Figure 7c, the bright and well-defined diffractions as well as no change of the SAED patterns at different regions of an individual microwire prove the single-crystal nature of the whole wire, demonstrating the good crystallinity of **5b**. According to the SAED diffraction patterns, a repeating unit of 7.2 Å along the crystal growth direction is observed. This value is much smaller than that of the molecular width and length, indicating that the molecular packing orientation of **5b** is probably along the crystal growth direction. The good crystallinity of **5b** may be correlated to its large π-framework without any steric hindrance at the periphery.

To investigate the electron-transporting properties of these B←N-containing polyarenes, we fabricated the OFET devices based on the single-crystal microwires of **5b**. The SC-OFET devices with a bottom-gate/top-contact (BG/TC) configuration were fabricated using the "organic ribbon mask" method.[20] Gold source and drain electrodes were deposited on an individual microwire via thermal evaporation (Figure 7d). The optical microscopy image of one typical device is

DOI: 10.1021/jacs.9b09640
J. Am. Chem. Soc. 2019, 141, 17015−17021

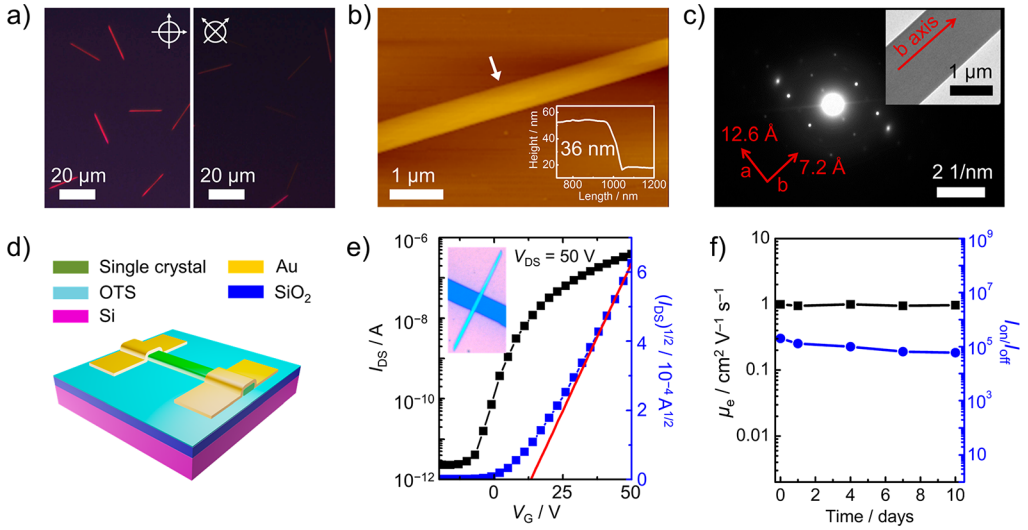

Figure 7. (a) Polarized optical microscopy images of the single-crystal microwires with rotations of 0° and 45°. (b) AFM image with the thickness analysis and (c) SAED pattern with a TEM image of a typical single-crystal microwire. (d) Schematic device structure of the BG/TC SC-OFETs. (e) Transfer curves of the SC-OFET device based on **5b** with its optical microscopy image. (f) Stability of the SC-OFET device in air at room temperature.

shown in the inset of Figure 7e. The transfer and output characteristics of the device measured under ambient conditions are provided in Figure 7e and Figure S15. The SC-OFET device exhibits the unipolar n-type behavior. A highest electron mobility of 1.60 $cm^2 V^{-1} s^{-1}$ (average of 20 devices: 1.03 ± 0.21 $cm^2 V^{-1} s^{-1}$) with an on/off current ratio of 10^5–10^6 and a threshold voltage of 14 V was obtained (Figure S16). Furthermore, the excellent ambient stability of the SC-OFET device of **5b** was demonstrated. Figure 7f shows the typical curves of performance versus storage time. Less than 5% degradation in electron mobility was observed after storing the device in air for 10 days. Therefore, the electron-transporting properties of **5b** are greatly improved in comparison to those of the reported dibenzo-azaacene containing two B←N units. It is ascribed to the significantly enhanced electron affinity and good crystallinity of **5b**, which facilitate electron injection and transport and improve air stability. To the best of our knowledge, this is the first time that electron mobility higher than 1 $cm^2 V^{-1} s^{-1}$ was obtained for organoboron compounds. B←N-containing polyarenes thus represent a new kind of high-performance n-type organic semiconductors.

CONCLUSIONS

In conclusion, we have synthesized two π-conjugated polyarenes incorporated with four B←N units through one-pot multifold borylation cyclization reaction. The incorporation of multiple B←N units significantly impacts their electronic structures and properties. **QBNA** has a LUMO energy level as low as −4.58 eV, illustrating its remarkably high electron affinity. Moreover, **QBNA** shows good crystallinity despite its curved configuration. The SC-OFET devices based on **QBNA** display unipolar n-type behavior with an electron mobility of 1.60 $cm^2 V^{-1} s^{-1}$ and excellent ambient stability. This study thus experimentally proves the high electron affinity and high electron mobility of organoboron compounds. Furthermore, this study provides a design strategy for π-systems with high electron affinity based on organoboron chemistry, which can be applied to the construction of other electronic materials.

ASSOCIATED CONTENT

Supporting Information

The Supporting Information is available free of charge on the ACS Publications website at DOI: 10.1021/jacs.9b09640.

Experimental details, thermal and photophysical properties, and theoretical calculations of **5a** and **5b**, as well as the SC-OFET device fabrications and characterizations of **5b** (PDF)

AUTHOR INFORMATION

Corresponding Authors

*chuandong.dou@ciac.ac.cn
*dhl522@iccas.ac.cn
*liujun@ciac.ac.cn

ORCID

Huanli Dong: 0000-0002-5698-5369
Jun Liu: 0000-0003-1487-0069

Notes

The authors declare no competing financial interest.

ACKNOWLEDGMENTS

This work was supported by the National Natural Science Foundation of China (Nos. 21822507, 21625403, and 51725304) and National Key Research and Development Program of China (No. 2018YFE0100600) founded by MOST. C.D. also thanks Youth Innovation Promotion Association of Chinese Academy of Sciences (No. 2017265) and State Key Laboratory of Supramolecular Structure and Materials in Jilin University (No. sklssm201905).

REFERENCES

(1) (a) Batley, M.; Lyons, L. E. Electron Affinities of Organic Molecules. *Nature* **1962**, *196*, 573–574. (b) Pritchard, H. O. The Determination of Electron Affinities. *Chem. Rev.* **1953**, *52*, 529–563.

DOI: 10.1021/jacs.9b09640
J. Am. Chem. Soc. 2019, 141, 17015–17021

(2) (a) Anthony, J. E.; Facchetti, A.; Heeney, M.; Marder, S. R.; Zhan, X. n-Type Organic Semiconductors in Organic Electronics. *Adv. Mater.* **2010**, *22*, 3876−3892. (b) Li, C.; Liu, M.; Pschirer, N. G.; Baumgarten, M.; Müllen, K. Polyphenylene-Based Materials for Organic Photovoltaics. *Chem. Rev.* **2010**, *110*, 6817−6855. (c) Zhang, G.; Zhao, J.; Chow, P. C. Y.; Jiang, K.; Zhang, J.; Zhu, Z.; Zhang, J.; Huang, F.; Yan, H. Nonfullerene Acceptor Molecules for Bulk Heterojunction Organic Solar Cells. *Chem. Rev.* **2018**, *118*, 3447−3507. (d) Lu, Y.; Wang, J.-Y.; Pei, J. Strategies To Enhance the Conductivity of n-Type Polymer Thermoelectric Materials. *Chem. Mater.* **2019**, *31*, 6412−6423.

(3) (a) Tang, M. L.; Oh, J. H.; Reichardt, A. D.; Bao, Z. Chlorination: A General Route toward Electron Transport in Organic Semiconductors. *J. Am. Chem. Soc.* **2009**, *131*, 3733−3740. (b) Guo, X.; Facchetti, A.; Marks, T. J. Imide- and Amide-Functionalized Polymer Semiconductors. *Chem. Rev.* **2014**, *114*, 8943−9021. (c) Bunz, U. H. F.; Engelhart, J. U.; Lindner, B. D.; Schaffroth, M. Large N-Heteroacenes: New Tricks for Very Old Dogs? *Angew. Chem., Int. Ed.* **2013**, *52*, 3810−3821. (d) Feng, J.; Jiang, W.; Wang, Z. Synthesis and Application of Rylene Imide Dyes as Organic Semiconducting Materials. *Chem. - Asian J.* **2018**, *13*, 20−30. (e) Miao, Q. Ten Years of N-Heteropentacenes as Semiconductors for Organic Thin-Film Transistors. *Adv. Mater.* **2014**, *26*, 5541−5549.

(4) (a) Zhao, Y.; Guo, Y.; Liu, Y. 25th Anniversary Article: Recent Advances in n-Type and Ambipolar Organic Field-Effect Transistors. *Adv. Mater.* **2013**, *25*, 5372−5391. (b) Wang, C.; Dong, H.; Hu, W.; Liu, Y.; Zhu, D. Semiconducting π-Conjugated Systems in Field-Effect Transistors: A Material Odyssey of Organic Electronics. *Chem. Rev.* **2012**, *112*, 2208−2267.

(5) (a) Lv, A.; Puniredd, S. R.; Zhang, J.; Li, Z.; Zhu, H.; Jiang, W.; Dong, H.; He, Y.; Jiang, L.; Li, Y.; Pisula, W.; Meng, Q.; Hu, W.; Wang, Z. High Mobility, Air Stable, Organic Single Crystal Transistors of an n-Type Diperylene Bisimide. *Adv. Mater.* **2012**, *24*, 2626−2630. (b) Chu, M.; Fan, J.-X.; Yang, S.; Liu, D.; Ng, C. F.; Dong, H.; Ren, A.-M.; Miao, Q. Halogenated Tetraazapentacenes with Electron Mobility as High as 27.8 $cm^2 V^{-1} s^{-1}$ in Solution-Processed n-Channel Organic Thin-Film Transistors. *Adv. Mater.* **2018**, *30*, 1803467. (c) Gao, X.; Hu, Y. Development of n-Type Organic Semiconductors for Thin Film Transistors: A Viewpoint of Molecular Design. *J. Mater. Chem. C* **2014**, *2*, 3099−3117.

(6) (a) He, T.; Stolte, M.; Würthner, F. Air-Stable n-Channel Organic Single Crystal Field-Effect Transistors Based on Microribbons of Core-Chlorinated Naphthalene Diimide. *Adv. Mater.* **2013**, *25*, 6951−6955. (b) Soeda, J.; Uemura, T.; Mizuno, Y.; Nakao, A.; Nakazawa, Y.; Facchetti, A.; Takeya, J. High Electron Mobility in Air for N,N′-1*H*,1*H*-Perfluorobutyldicyanoperylene Carboxydi-imide Solution-Crystallized Thin-Film Transistors on Hydrophobic Surfaces. *Adv. Mater.* **2011**, *23*, 3681−3685. (c) Xue, G.; Wu, J.; Fan, C.; Liu, S.; Huang, Z.; Liu, Y.; Shan, B.; Xin, H. L.; Miao, Q.; Chen, H.; Li, H. Boosting the Electron Mobility of Solution-Grown Organic Single Crystals via Reducing the Amount of Polar Solvent Residues. *Mater. Horiz.* **2016**, *3*, 119−123. (d) Xu, X.; Yao, Y.; Shan, B.; Gu, X.; Liu, D.; Liu, J.; Xu, J.; Zhao, N.; Hu, W.; Miao, Q. Electron Mobility Exceeding 10 $cm^2 V^{-1} s^{-1}$ and Band-Like Charge Transport in Solution-Processed n-Channel Organic Thin-Film Transistors. *Adv. Mater.* **2016**, *28*, 5276−5283. (e) Dou, J.-H.; Zheng, Y.-Q.; Yao, Z.-F.; Yu, Z.-A.; Lei, T.; Shen, X.; Luo, X.-Y.; Sun, J.; Zhang, S.-D.; Ding, Y.-F.; Han, G.; Yi, Y.; Wang, J.-Y.; Pei, J. Fine-Tuning of Crystal Packing and Charge Transport Properties of BDOPV Derivatives through Fluorine Substitution. *J. Am. Chem. Soc.* **2015**, *137*, 15947−15956. (f) Zhang, C.; Zang, Y.; Gann, E.; McNeill, C. R.; Zhu, X.; Di, C.-A.; Zhu, D. Two-Dimensional π-Expanded Quinoidal Terthiophenes Terminated with Dicyanomethylenes as n-Type Semiconductors for High-Performance Organic Thin-Film Transistors. *J. Am. Chem. Soc.* **2014**, *136*, 16176−16184.

(7) (a) Hirai, M.; Tanaka, N.; Sakai, M.; Yamaguchi, S. Structurally Constrained Boron-, Nitrogen-, Silicon-, and Phosphorus-Centered Polycyclic π-Conjugated Systems. *Chem. Rev.* **2019**, *119*, 8291−8331. (b) Ren, Y.; Jäkle, F. Merging Thiophene with Boron: New Building Blocks for Conjugated Materials. *Dalton Trans.* **2016**, *45*, 13996−14007. (c) Frath, D.; Massue, J.; Ulrich, G.; Ziessel, R. Luminescent Materials: Locking π-Conjugated and Heterocyclic Ligands with Boron(III). *Angew. Chem., Int. Ed.* **2014**, *53*, 2290−2310. (d) Melleruup, S. K.; Wang, S. Boron-Based Stimuli Responsive Materials. *Chem. Soc. Rev.* **2019**, *48*, 3537−3549. (e) Lorbach, A.; Hübner, A.; Wagner, M. Aryl(hydro)boranes: Versatile Building Blocks for Boron-Doped π-Electron Materials. *Dalton Trans.* **2012**, *41*, 6048−6063. (f) Campbell, P. G.; Marwitz, A. J. V.; Liu, S.-Y. Recent Advances in Azaborine Chemistry. *Angew. Chem., Int. Ed.* **2012**, *51*, 6074−6092.

(8) (a) Ji, L.; Griesbeck, S.; Marder, T. B. Recent Developments in and Perspectives on Threecoordinate Boron Materials: A Bright Future. *Chem. Sci.* **2017**, *8*, 846−863. (b) Kondo, Y.; Yoshiura, K.; Kitera, S.; Nishi, H.; Oda, S.; Gotoh, H.; Sasada, Y.; Yanai, M.; Hatakeyama, T. Narrowband Deep-Blue Organic Light-Emitting Diode Featuring An Organoboron-Based Emitter. *Nat. Photonics* **2019**, *13*, 678−682. (c) Stennett, T. E.; Bissinger, P.; Griesbeck, S.; Ullrich, S.; Krummenacher, I.; Auth, M.; Sperlich, A.; Stolte, M.; Radacki, K.; Yao, C.-J.; Würthner, F.; Steffen, A.; Marder, T. B.; Braunschweig, H. Near-Infrared Quadrupolar Chromophores Combining Three-Coordinate Boron-Based Superdonor and Superacceptor Units. *Angew. Chem., Int. Ed.* **2019**, *58*, 6449−6454.

(9) (a) Noda, T.; Shirota, Y. 5,5′-Bis(dimesitylboryl)-2,2′-bithiophene and 5,5″-Bis(dimesitylboryl)-2,2′:5′,2″-terthiophene as a Novel Family of Electron-Transporting Amorphous Molecular Materials. *J. Am. Chem. Soc.* **1998**, *120*, 9714−9715. (b) Caruso, A., Jr.; Siegler, M. A.; Tovar, J. D. Synthesis of Functionalizable Boron-Containing π-Electron Materials that Incorporate Formally Aromatic Fused Borepin Rings. *Angew. Chem., Int. Ed.* **2010**, *49*, 4213−4217. (c) Zhao, R.; Dou, C.; Liu, J.; Wang, L. An Alternating Polymer of Two Building Blocks Based on B←N Unit: Non-fullerene Acceptor for Organic Photovoltaics. *Chin. J. Polym. Sci.* **2017**, *35*, 198−206. (d) Crossley, D. L.; Cade, I. A.; Clark, E. R.; Escande, A.; Humphries, M. J.; King, S. M.; Vitorica-Yrezabal, I.; Ingleson, M. J.; Turner, M. L. Enhancing Electron Affinity and Tuning Band Gap in Donor-Acceptor Organic Semiconductors by Benzothiadiazole Directed C−H Borylation. *Chem. Sci.* **2015**, *6*, 5144−5151.

(10) (a) Farrell, J. M.; Mützel, C.; Bialas, D.; Rudolf, M.; Menekse, K.; Krause, A.-M.; Stolte, M.; Würthner, F. Tunable Low-LUMO Boron-Doped Polycyclic Aromatic Hydrocarbons by General One-Pot C−H Borylations. *J. Am. Chem. Soc.* **2019**, *141*, 9096−9104. (b) Kushida, T.; Shirai, S.; Ando, N.; Okamoto, T.; Ishii, H.; Matsui, H.; Yamagishi, M.; Uemura, T.; Tsurumi, J.; Watanabe, S.; Takeya, J.; Yamaguchi, S. Boron-Stabilized Planar Neutral π-Radicals with Well-Balanced Ambipolar Charge-Transport Properties. *J. Am. Chem. Soc.* **2017**, *139*, 14336−14339. (c) Yin, X.; Liu, K.; Ren, Y.; Lalancette, R. A.; Loo, Y.-L.; Jäkle, F. Pyridalthiadiazole Acceptor-Functionalized Triarylboranes with Multi-Responsive Optoelectronic Characteristics. *Chem. Sci.* **2017**, *8*, 5497−5505. (d) Min, Y.; Dou, C.; Tian, H.; Liu, J.; Wang, L. A Disk-Type Polyarene Containing Four B←N Units. *Chem. Commun.* **2019**, *55*, 3638−3641. (e) Matsuo, K.; Saito, S.; Yamaguchi, S. Photodissociation of B−N Lewis Adducts: A Partially Fused Trinaphthylborane with Dual Fluorescence. *J. Am. Chem. Soc.* **2014**, *136*, 12580−12583.

(11) (a) Wakamiya, A.; Taniguchi, T.; Yamaguchi, S. Intramolecular B−N Coordination as a Scaffold for Electron-Transporting Materials: Synthesis and Properties of Boryl-Substituted Thienylthiazoles. *Angew. Chem., Int. Ed.* **2006**, *45*, 3170−3173. (b) Dou, C.; Liu, J.; Wang, L. Conjugated Polymers Containing B←N Unit as Electron Acceptors for All-Polymer Solar Cells. *Sci. China: Chem.* **2017**, *60*, 450−459. (c) Li, P.; Chan, H.; Lai, S.-L.; Ng, M.; Chan, M.-Y.; Yam, V. W.-W. Four-Coordinate Boron Emitters with Tridentate Chelating Ligand for Efficient and Stable Thermally Activated Delayed Fluorescence Organic Light-Emitting Devices. *Angew. Chem., Int. Ed.* **2019**, *58*, 9088−9094.

(12) Min, Y.; Dou, C.; Tian, H.; Geng, Y.; Liu, J.; Wang, L. n-Type Azaacenes Containing B←N Units. *Angew. Chem., Int. Ed.* **2018**, *57*, 2000−2004.

DOI: 10.1021/jacs.9b09640
J. Am. Chem. Soc. 2019, 141, 17015−17021

(13) Figueira-Duarte, T. M.; Müllen, K. Pyrene-Based Materials for Organic Electronics. *Chem. Rev.* **2011**, *111*, 7260−7314.
(14) (a) Yoshii, R.; Hirose, A.; Tanaka, K.; Chujo, Y. Functionalization of Boron Diiminates with Unique Optical Properties: Multicolor Tuning of Crystallization-Induced Emission and Introduction into the Main Chain of Conjugated Polymers. *J. Am. Chem. Soc.* **2014**, *136*, 18131−18139. (b) Qiu, F.; Zhang, F.; Tang, R.; Fu, Y.; Wang, X.; Han, S.; Zhuang, X.; Feng, X. Triple Boron-Cored Chromophores Bearing Discotic 5,11,17-Triazatrinaphthylene-Based Ligands. *Org. Lett.* **2016**, *18*, 1398−1401.
(15) Cui, X.; Xiao, C.; Winands, T.; Koch, T.; Li, Y.; Zhang, L.; Doltsinis, N. L.; Wang, Z. Hexacene Diimides. *J. Am. Chem. Soc.* **2018**, *140*, 12175−12180.
(16) (a) Segawa, Y.; Ito, H.; Itami, K. Structurally Uniform and Atomically Precise Carbon Nanostructures. *Nat. Rev. Mater.* **2016**, *1*, 15002. (b) Pun, S. H.; Miao, Q. Toward Negatively Curved Carbons. *Acc. Chem. Res.* **2018**, *51*, 1630−1642. (c) Ball, M.; Zhong, Y.; Wu, Y.; Schenck, C.; Ng, F.; Steigerwald, M.; Xiao, S.; Nuckolls, C. Contorted Polycyclic Aromatics. *Acc. Chem. Res.* **2015**, *48*, 267−276. (d) Liu, J.; Ma, J.; Zhang, K.; Ravat, P.; Machata, P.; Avdoshenko, S.; Hennersdorf, F.; Komber, H.; Pisula, W.; Weigand, J. J.; Popov, A. A.; Berger, R.; Müllen, K.; Feng, X. π-Extended and Curved Antiaromatic Polycyclic Hydrocarbons. *J. Am. Chem. Soc.* **2017**, *139*, 7513−7521.
(17) (a) Liu, K.; Lalancette, R. A.; Jäkle, F. B−N Lewis Pair Functionalization of Anthracene: Structural Dynamics, Optoelectronic Properties, and O_2 Sensitization. *J. Am. Chem. Soc.* **2017**, *139*, 18170−18173. (b) Liu, K.; Lalancette, R. A.; Jäkle, F. Tuning the Structure and Electronic Properties of B−N Fused Dipyridylanthracene and Implications on the Self-Sensitized Reactivity with Singlet Oxygen. *J. Am. Chem. Soc.* **2019**, *141*, 7453−7462.
(18) (a) Seifert, S.; Shoyama, K.; Schmidt, D.; Würthner, F. An Electron-Poor C64 Nanographene by Palladium-Catalyzed Cascade C−C Bond Formation: One-Pot Synthesis and Single-Crystal Structure Analysis. *Angew. Chem., Int. Ed.* **2016**, *55*, 6390−6395. (b) Cortizo-Lacalle, D.; Mora-Fuentes, J. P.; Strutynski, K.; Saeki, A.; Melle-Franco, M.; Mateo-Alonso, A. Monodisperse N-Doped Graphene Nanoribbons Reaching 7.7 Nanometers in Length. *Angew. Chem., Int. Ed.* **2018**, *57*, 703−708.
(19) (a) Ni, Y.; Lee, S.; Son, M.; Aratani, N.; Ishida, M.; Samanta, A.; Yamada, H.; Chang, Y.-T.; Furuta, H.; Kim, D.; Wu, J. A Diradical Approach towards BODIPY-Based Dyes with Intense Near-Infrared Absorption around λ = 1100 nm. *Angew. Chem., Int. Ed.* **2016**, *55*, 2815−2819. (b) Fischer, G. M.; Daltrozzo, E.; Zumbusch, A. Selective NIR Chromophores: Bis(Pyrrolopyrrole) Cyanines. *Angew. Chem., Int. Ed.* **2011**, *50*, 1406−1409.
(20) (a) Jiang, L.; Gao, J.; Wang, E.; Li, H.; Wang, Z.; Hu, W.; Jiang, L. Organic Single-Crystalline Ribbons of a Rigid ″H″-type Anthracene Derivative and High-Performance, Short-Channel Field-Effect Transistors of Individual Micro/Nanometer-Sized Ribbons Fabricated by an ″Organic Ribbon Mask″ Technique. *Adv. Mater.* **2008**, *20*, 2735−2740. (b) Zhang, X.; Dong, H.; Hu, W. Organic Semiconductor Single Crystals for Electronics and Photonics. *Adv. Mater.* **2018**, *30*, 1801048.

DOI: 10.1021/jacs.9b09640
J. Am. Chem. Soc. 2019, 141, 17015−17021